Springer

KSME

Journal of Mechanical Science and Technology 30 (11) (2016) 5167~5182
www.springerlink.com/content/1738-494x(Print)/1976-3824(Online)
DOI 10.1007/s12206-016-1035-3

Experimental study on cascaded attitude angle control of a multi-rotor unmanned aerial vehicle with the simple internal model control method †

Jun-Beom Song[1], Young-Seop Byun[2], Jin-Seok Jeong[2], Jeong Kim[2] and Beom-Soo Kang[2,*]

[1]*Department of Aviation Maintenance, Dongwon Institute of Science and Technology, Yangsan 50578, Korea*
[2]*Department of Aerospace Engineering, Pusan National University, Busan 609-735, Korea*

(Manuscript Received October 6, 2014; Revised November 30, 2015; Accepted June 30, 2016)

Abstract

This paper proposes a cascaded control structure and a method of practical application for attitude control of a multi-rotor Unmanned aerial vehicle (UAV). The cascade control, which has tighter control capability than a single-loop control, is rarely used in attitude control of a multi-rotor UAV due to the input-output relation, which is no longer simply a set-point to Euler angle response transfer function of a single-loop PID control, but there are multiply measured signals and interactive control loops that increase the complexity of evaluation in conventional way of design. However, it is proposed in this research a method that can optimize a cascade control with a primary and secondary loops and a PID controller for each loop. An investigation of currently available PID-tuning methods lead to selection of the Simple internal model control (SIMC) method, which is based on the Internal model control (IMC) and direct-synthesis method. Through the analysis and experiments, this research proposes a systematic procedure to implement a cascaded attitude controller, which includes the flight test, system identification and SIMC-based PID-tuning. The proposed method was validated successfully from multiple applications where the application to roll axis lead to a PID-PID cascade control, but the application to yaw axis lead to that of PID-PI.

Keywords: Cascade control; Simple internal model control (SIMC); Quad rotor; Multi-rotor; Unmanned aerial vehicle; PID control; Frequency sweep method; System identification; Attitude control

1. Introduction

In recent years, more and more Unmanned aerial vehicles (UAV) were built. From 2011 to 2020, the total number of drones that will be built around the world in this period is expected to exceed 27000. Among those UAVs, 81 % are small or mini UAVs, and the number of UAVs in toy or hobby market is not even included in the market survey [1]. It is inevitable that more small UAVs will be seen in the commercial market when considering a new major civil UAV projects under way for various services by Amazon, Google, and many other companies. Therefore, it will be beneficial to current industry of commercial UAVs, and to individuals who are trying to fly one as a hobby, if an established method of flight control is provided.

It is already widely used in the industry, the Proportional-integral-derivative (PID) control, and a simple rule-based PID tuning method. A more sophisticated modern control methods were rarely used when the PID controller have already provided the simplicity and control performance for many decades. It has been seen that more than 95 % of industrial control loops are using the PID [2] because the properly designed PID control gives similar or even better performance than sophisticated non-linear controllers such as Fuzzy logic [3]. Therefore, most of commercial Flight control computers (FCC) provide a PID control and a recommended gain values that an individuals can tune to the specific configuration of a target platform of a UAV [4, 5].

Meanwhile, a cascade control, which is an advanced extension of PID control, has been used in the process control in variety of industries including a motor control, chemical flow control, boiler control, engine throttle control, and etc [6]. The cascade control can improve the response time and reduce load disturbance when there are multiple measureable signals for one control variable. In general, the cascade control has a primary loop and a secondary loop, where the faster dynamics involved in the secondary loop provides quicker response and tight feedback around the load disturbance while the primary loop determines the tracking performance in a relatively slower dynamics [7].

Surprisingly, no commercial FCCs provided a cascade control structure to attitude control of a UAV - i.e., roll, pitch and yaw angle control. When the target platform of UAV is

*Corresponding author. Tel.: +82 51 510 2310, Fax.: +82 51 513 3760
E-mail address: bskang@pusan.ac.kr
† Recommended by Associate Editor Deok Jin Lee
© KSME & Springer 2016

different from the one used by the manufacturer of the commercial FCC, the user will either have to suffer from poor performance or have to tune gain values with a rule-based empirical tuning procedure - i.e., by trial-and-error. Therefore, the minimization of complexity for general user will be the main reason why commercial FCCs are usually provided with a single-loop PID control [4, 5].

Even in the research field, the cascade control is rarely used for attitude control of a UAV. Taking it into consideration of how widely the cascade structure has been adopted in various systems, it is surprising how little the number of literatures is found for attitude control of a UAV by cascade control. However, the most notable research was done by Czyba and Szafranski [8]. They proposed a cascade control system for attitude control where the secondary loop provides angular stabilization and the primary loop provides tracking performance. Their approach consolidates the basic principles of the cascade control into the attitude control of a multi-rotor, where the number of signals is to be limited up to measurable signals, and the distributed functionality of each loops – i.e., the stabilization by the angular velocity control of secondary loop and the angular tracking performance by the primary loop. However, their concern was a structure of modified PID control to compare the performance between parallel-form PID, PI-D and I-PD structure with gradient-decent optimization method - not the tuning method nor the tighter control by cascade control. Godbolt and Lynch [9] also showed another example of a cascade control to compensate small body force in helicopter control. However, their interest was to compensate the coupling between the inputs to rotational and translational dynamics due to the so-called 'small body force' which is mostly an issue for a single rotor helicopter with dynamically coupled tail rotor and main rotor.

It is noteworthy to compare with the motor control that has been using a cascade control where the typical system has three cascaded loops [10]. The innermost, the intermediate, and the outer loops each has feedback loop of current, angular velocity, and angular position. Therefore, separate measurements of the electric current, rotational speed, and absolute position are required. However, in case of the attitude control of a UAV, the measurement is generally provided from 3-axis gyro for angular velocity and the Euler angle is provided from integrated value of angular velocity which is Kalman filtered with 3-axis accelerometers, and 3-axis magnetometers. Although more components are incorporated, it is the default Attitude-heading reference system (AHRS) that is always required in a UAV. In other words, the secondary measured variable for cascaded attitude control is provided with no additional cost [8].

Therefore, this research stems from the lack of research, the tighter control, the better load disturbance performance, and the minimized cost required to implement the cascade control for attitude control of a UAV, thus benefiting in the current industrial field of UAV systems.

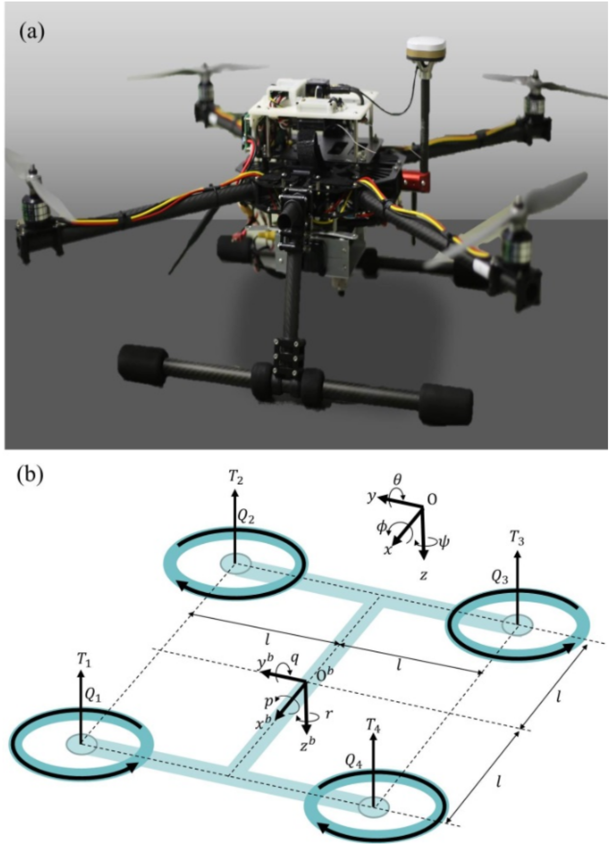

Fig. 1. (a) The target quad-rotor platform; (b) general configuration.

The main goal of this research is to find a system identification method and to apply an analytic PID-tuning method, and conclusively, a procedure that is easy to apply for a cascaded attitude control. The scope, however, was limited to a Vertical take-off and landing (VTOL) UAV because its hovering and VTOL capability makes it an ideal choice for various missions, and thus it is expected to be more prevalent in current UAV industry than any other configuration such as a conventional fixed-wing, wing-body, flapping wing, and etc [1]. Among the VOTL UAVs, a quad-rotor platform, which is the most general configuration of multi-rotor platforms, was chosen for the exemplary application because it is impossible to fly it in an open-loop control. In other words, it is impossible to fly a quad-rotor by fully manual control, and the attitude control is more important in a quad-rotor platform than that in a manually controllable helicopter [11].

In this paper, the procedure and strategy of applying the cascade control is firstly presented based on the general issues of problems that arise when the cascaded attitude control is to be applied in a UAV. The investigation of currently available PID-tuning methods lead to selection of the Simple internal model control (SIMC) method. From the next section, since this method is trying to develop a practical method that can be applied at the industrial field, all procedures are evaluated from the real application in a quad-rotor platform.

2. Procedure of tuning a cascaded attitude control

2.1 Background knowledge

This section provides a general description of the quad-rotor platform and important assumptions and considerations for current application. The quad-rotor, which is one of the multi-rotor configurations, has four motors fixed at four corners of its body. The most general type of a small quad-rotor was chosen as the target platform, which is shown in the Figs. 1(a) and (b). Further descriptions for 6-Degree of freedom (6-DOF) equation of motion is not required to be presented from this paper because it is already widely developed by many researchers [8, 11, 12], but only a few elements to describe the current application will be treated.

It is shown in Fig. 1(b) the configuration of the motor thrusts $T_1 \sim T_4$, torques $Q_1 \sim Q_4$, and symmetric moment arm l. The body fixed reference frame *B*: (O^b, x^b, y^b, z^b) and the local level inertial reference frame *W*: (*O, x, y, z*) are also shown where the x^b axis points towards the middle of motor #1 and #4. It is also possible to use the x^b axis to point toward the motor #1, but there is no fundamental difference, and it is freely switchable.

The quad rotor platform used in this paper has 0.295 m length for the moment arm l, and takeoff-weight of 3.9 kg (38.3 N). The maximum thrust for each set of the motor is around 21 N using a propeller with 33 cm length, which leads to total of 85 N maximum lifting thrust. As commercial FCCs usually provide high sampling and control rate, the current exemplary application was utilizing a self-developed FCC with 100 Hz data acquisition and attitude control while up to 400 Hz motor speed control was provided.

Throughout the paper, conventional terms of the aileron, elevator and rudders will be used. The aileron corresponds to the control signal to create rolling moment around the x^b axis. Similarly, the elevator corresponds to the control signal to create pitching moment around the y^b axis, and the rudder for yawing moment around the z^b axis. However, for convenience, the aileron, elevator and rudder will be normalized in -100 % ~ +100 % from the maximum control force available by the motors, and will be termed *AIL*, *ELE* and *RUD*, respectively. By normalizing the control variable, it is clear how much control force is used, and it is easier to apply the limitation at ±100 %. It is shown from the Appendix A.1. for more explanation of these control variables.

For overall design of control, there are two fundamental assumptions:

(a) Assumption of decoupled control input to response.

(b) Assumption of small angle.

The first assumption simply means that the roll, pitch and yaw controllers have no coupled state from *AIL*, *ELE* and *RUD* input, respectively, which result to a simple Single input single output (SISO) control design. This means, however, that the cross-product term of so-called ‘small body forces’ are ignored which is commonly neglected for SISO control design. From this basis, the full description of 6-DOF equations of motion is not noteworthy for SISO control design.

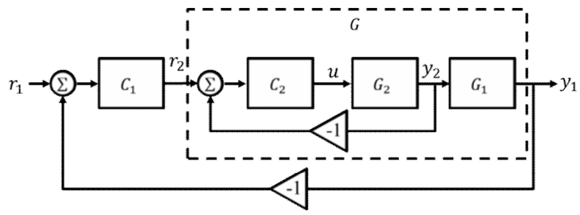

Fig. 2. General cascade control system.

The second assumption is to be described with a conversion matrix $\boldsymbol{C}$ that converts the Euler angular rate $\boldsymbol{\omega}$ to the body angular rate $\boldsymbol{\omega}^b$ as:

$$\boldsymbol{\omega}^b = \begin{bmatrix} p \\ q \\ r \end{bmatrix} = \boldsymbol{C} \begin{bmatrix} \dot{\phi} \\ \dot{\theta} \\ \dot{\psi} \end{bmatrix}, \quad \boldsymbol{\omega} = \begin{bmatrix} \dot{\phi} \\ \dot{\theta} \\ \dot{\psi} \end{bmatrix} = \boldsymbol{C}^{-1} \begin{bmatrix} p \\ q \\ r \end{bmatrix} \tag{1}$$

where

$$\boldsymbol{C} = \begin{bmatrix} 1 & 0 & -\sin\theta \\ 0 & \cos\phi & \sin\phi\cos\theta \\ 0 & -\sin\phi & \cos\phi\cos\theta \end{bmatrix},$$
$$\boldsymbol{C} = \begin{bmatrix} 1 & \sin\phi\tan\theta & \cos\phi\tan\theta \\ 0 & \cos\phi & -\sin\phi \\ 0 & \sin\phi/\cos\theta & \cos\phi/\cos\theta \end{bmatrix}. \tag{2}$$

From Eqs. (1) and (2), p, q and r are body frame angular velocities around x^b, y^b and z^b axes, respectively, and ϕ, θ and ψ are Euler angles of roll, pitch and yaw, respectively. Therefore, from the second assumption, the conversion matrix $\boldsymbol{C}$ becomes an identity matrix of 3×3 size, and $\boldsymbol{\omega} \approx \boldsymbol{\omega}^b$.

2.2 Definition of the problem

In this paper, a cascade control is defined with the structure as shown in Fig. 2, where C_1 and C_2 are the primary and secondary control with negative feedback, respectively. G_1 and G_2 are the physical process model where the intermediate secondary variable can be measured from G_2. The set-point r_1 is given for the primary measured variable y_1, and the primary loop control C_1 yields the set-point r_2 for the secondary measured variable y_2. It is known as a fact that the cascade control improves the set-point response because the secondary loop is operating with faster dynamics and higher gain which also leads to improved load disturbance [10]. Using the secondary measured variable as angular velocity, the cascaded attitude control – that is, Euler angle control - can be achieved without any additional sensor or calculation from the view point of a UAV. For such a small quad-rotor UAV as it was shown from Fig. 1, where the poorly streamlined structure of a UAV with extruded payloads increases the suscepti-

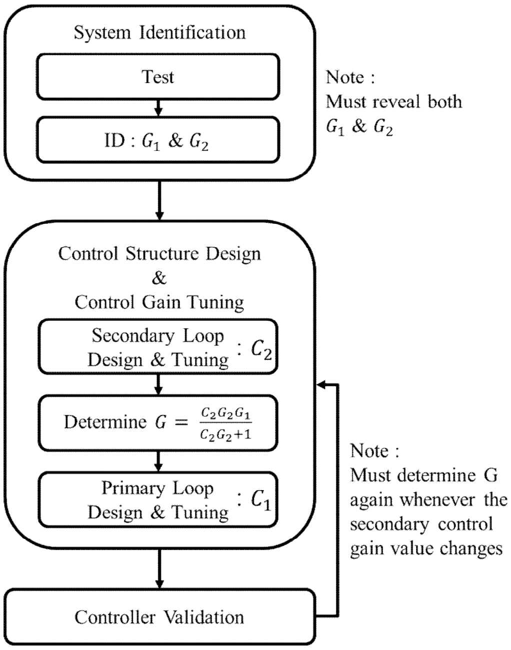

Fig. 3. General procedure of a cascade control design.

bility to gust, the cascaded attitude control will provide a better performance [13-15].

However, when compared with a more straight-forward single-loop control, the major drawback of the cascade control systems is the complexity created by multiple control loops. If the primary controller C_1 is to be designed, the process model is not simply G_1G_2 but has a different form as:

$$G = \frac{C_2G_2G_1}{C_2G_2+1} \tag{3}$$

where the $\boldsymbol{G}$ is introduced to indicate the process model for primary controller, and it is the main reason for the increased complexity. For example, a time-delayed model with η seconds of effective time-delay will suffer from the complexity caused by $e^{-\eta s}$ term in G_1 and G_2. Therefore, a generalized process is required for cascaded attitude control for modeling of the process model $\boldsymbol{G}$ for primary control.

Another problem of complexity is the decision for a repeated use of integral control and derivative control. With examples of PI-PD and PID-P, it is sometimes avoided to use repeated I and D control [10, 16, 17]. It is seemingly wise to avoid the repeated use in order to avoid wind-up and high frequency derivative problem, however, there should be some analytical approach for choosing the structure from a PID control.

Since the increased numbers of gain values obstruct the optimal gain-tuning by a simple rule-based empirical tuning without a process model, a general procedure of a cascade control design can be summarized with a process diagram defined in Fig. 3 that involves modeling. It is a common practice to perform a system identification (ID) process for a control design to determine the process model [18, 19]. The design and tuning of a controller is the next step which is followed by a validation process. It is clearer from this process diagram that the complexity of a cascade control may hinder the overall process as the following summary:

(1) System ID safety problem – The 'system identification' process must reveal both the fast dynamics of G_2 and slow dynamics of G_1, where G_2 may require a high-frequency actuator input that may have a safety issue in a certain UAV and in a particular dynamic mode.

(2) Model uncertainty problem – For example, it seems clear that the physical relation of Euler angles and angular velocity leads to $G_1 = 1/s$, however, the identified G_1G_2 may not have $1/s$ term at all, due to noise that contaminated the flight data.

(3) Complex $\boldsymbol{G}$ problem – During the 'control structure design & control gain tuning' process, actual process model for the primary controller is composed of G_1 and feedback loop of C_2 and G_2 which is not easy to evaluate. Moreover, due to the interacting structure of the $\boldsymbol{G}$ with the secondary controller C_2, $\boldsymbol{G}$ has to be determined again any time C_2 is changed.

(4) PID structure problem – What will be the optimized structure for interacting C_1 and C_2 is not easy to analyze especially when the complex structure of $\boldsymbol{G}$ is combined.

From the 'test' procedure inside the 'system identification' block, by using an actuating input that can derive dynamic response from the system, a time-domain input and output data can be acquired. However, for a flying vehicle, this test is most likely to be performed in air if no ground testing jig is incorporated, and if the flying vehicle has less stability or unstable, additional controller should be added to ensure the safety. Even if a ground testing jig is used, the actual response in air may differ from the response on ground due to different mass, center of gravity, ground effect, and etc. What should be the input signal is also a problem. Usual inputs include a doublet, 3-2-1-1, sine wave sweep and rectangular on/off relay switch [20, 21]. Whatever the input signal, it should be able to derive the required knowledge of the dynamic model. Therefore, the first and the second issues of the summarized problems have to be considered.

The third and the fourth issues are already described before the summary. It is only clearer from the Fig. 3 that the increased complexity of a cascade control may require more time to incorporate optimal design.

2.3 Proposed procedure for cascaded attitude control

In order to tackle with the problems defined for cascade control, various PID tuning methods have been examined. In overall, PID tuning methods can be categorized into 5 methods. The conclusive remarks from the examination of the categories are presented below, and among them, the analytical methods were the best choice.

(1) Rule-based empirical tuning – Usually used for adjusting controller parameters to improve the performance during experiment, this method applies a simple set of rules that predicts the change of response from the change of controller gain values [10]. More sophisticated uses include an expert system that modifies the controller parameters based on cumulated data of human control history that captures repeatedly exhibited habits [22]. Another good example is a fuzzy logic [23]. However, the rule-based empirical tuning method is not considered a practical solution for a cascaded attitude control because the complexity of interacting structure may often incorporate many local minimum solutions away from the optimum point.

(2) Empirical formulae – Most well-known from the formulas devised by Ziegler and Nichols, the empirical formulae can be a good solution because of its simplicity. However, the empirical formulas are commonly known to have a problem to give poor robustness [24-26]. Therefore, it is not a recommendable choice for a small quad-rotor UAV.

(3) Frequency-domain methods – Although the frequency-domain methods have been a standard method for control system design commonly practiced by pole placement [10, 26], the fundamental drawback is that it requires extensive knowledge of process model over wide range of frequencies. Thus, it is not the problem of the tuning method, but the required system identification method that may cause a problem for a cascaded control system. However, more systematic approaches have been developed for integrating and unstable processes to be applied to an auto-tuning adaptive PID controller [27]. Therefore, frequency-domain methods may still be a good solution if no other options are available.

(4) Optimization methods – Minimizing an integral performance criteria or H_∞ performance index [10, 26], these methods may have to be used ultimately. However, the problem at this stage is that there is no determined criteria or performance index for a cascaded attitude control for small UAV yet. Moreover, optimization methods themselves does not provide logical solutions to the problems defined for the cascade control system, but it only gives an optimum set of gain values from a given performance criteria.

(5) Analytical methods – Unlike other methods, analytical methods evaluates the equations of process model and controller to provide a deterministic and logical way to derive controller parameters [10, 26]. Although Internal model control (IMC) is a well-known control design where the trade-off between nominal performance and robustness is explicitly addressed [28], direct-synthesis-based design method also gives an analytical determination of controller transfer function from a desired closed-loop transfer function [29, 30]. Conclusively, logical approaches of analytical methods may provide solutions to the cascade control system.

Among the analytical methods, the direct-synthesis-based design method and IMC were consolidated by Skogestad to a method called Simple internal model control (SIMC, or it may also refer to Skogestad-IMC) method [31-33]. In this method, a series form PID control expressed as Eq. (4) is used.

$$C(s) = K_c\left(\frac{\tau_I s+1}{\tau_I s}\right)\left(\tau_D s+1\right) = \frac{K_c}{\tau_I s}\left(\tau_I\tau_D s^2 + (\tau_I+\tau_D)s+1\right). \tag{4}$$

K_c, τ_I and τ_D are the controller gain, integral time and derivative time, respectively. A First-order time-delay (FOTD) or Second-order time-delay (SOTD) model is a basic process model. FOTD and SOTD are expressed as Eqs. (5) and (6), respectively.

$$G(s) = \frac{k}{\left(\tau_1 s+1\right)}e^{-\eta s} = \frac{k'}{\left(s+1/\tau_1\right)}e^{-\eta s} \tag{5}$$

$$G(s) = \frac{k}{\left(\tau_1 s+1\right)\left(\tau_2 s+1\right)}e^{-\eta s} = \frac{k'}{\left(s+1/\tau_1\right)\left(\tau_2 s+1\right)}e^{-\eta s}. \tag{6}$$

k is the plant gain, τ_1 the dominant lag time constant, τ_2 the second-order lag time constant, and η the effective time delay. The η is often called a dead-time, and it represents the pure delay of response from control input. Using the direct-synthesis for closed-loop transfer function, a desired closed-loop response of y from set-point y_{sp} is specified as:

$$\left(\frac{y}{y_{sp}}\right)_{desired} = \frac{1}{\tau_c s+1}e^{-\eta s}, \tag{7}$$

where the desired response is a simple first-order response with time constant τ_c and the same dead-time η from the process model. Analyzing the close-loop response by Taylor series approximation of time delay $e^{-\eta s} \approx 1-\eta s$, the gain values of Eq. (4) for the process model of Eq. (6) can be derived with following result – see Ref. [32].

$$K_c = \frac{1}{k}\frac{\tau_1}{\tau_c+\eta};\ \ \tau_I = \tau_1;\ \ \tau_D = \tau_2. \tag{8}$$

However, the SIMC method denotes that, although $\tau_I = \tau_1$ has an excellent set-point response, it has slow settling for a load disturbance. The final SIMC PID-tuning rule after analyzing the closed-loop characteristic polynomial $1+G(s)C(s)$, becomes:

$$K_c = \frac{1}{k}\frac{\tau_1}{\tau_c+\eta} = \frac{1}{k'}\frac{1}{\tau_c+\eta}, \tag{9a}$$

$$\tau_I = \min\{\tau_1, 4\left(\tau_c+\eta\right)\}, \tag{9b}$$

$$\tau_D = \tau_2, \tag{9c}$$

where the τ_c is the only tuning parameter. For practical application of SIMC in industrial usage, τ_c was recommended as:

$$\tau_c = \eta \,. \tag{9d}$$

The SIMC method simplifies the PID control tuning problem to a single-parameter tuning with a good initial value from Eq. (9d). Moreover, the SIMC method provides an analytical way to determine whether the controller should be PI or PID because Eq. (9c) explains the necessity of derivative control – i.e., if $\tau_2 \approx 0$, derivative control is unnecessary [32]. Therefore, the SIMC method was adopted for the current application.

Moreover, it was found from this research that Eq. (9a) of the SIMC method provided a good insight to the model because the ratio of τ_1 / k determines the control gain - not the absolute value for each of τ_1 and k. In system ID, depending on the analysis method, absolute values of τ_1 and k were ranging at a wide region. However, if $k' = \tau_1 / k$ values were the same, the value of K_c in Eq. (9a) could be determined. In addition, since τ_1 can be identified to have uncertain values, Eq. (9b) also serves as a good rule because τ_1 can be eliminated from PID tuning. Therefore, it can be viewed that the SIMC method does not require a very accurate process model, and lessens the problem of model uncertainty.

Using the SIMC method, the problem of complex $\boldsymbol{G}$ can be solved because it does not require accurate models of G_1 and G_2, but direct identification of linear behavior of the secondary loop transfer function $\boldsymbol{G}$ is enough to determine PID gain values. In other methods including the original IMC method, it is required to identify both G_1 and G_2, however, the direct-synthesis of the SIMC method already determined that the PID gain values are optimized at the chosen τ_c value.

Therefore, the only problem left for the cascade control is the safety issue during the identification of the fast G_2 dynamics. The safety issue depends on the stability of a target UAV platform. Generally, a small helicopter with a stabilizer bar or stabilizer paddle does not need any consideration but it only requires a skilled pilot who can manually fly the helicopter. However, a small quad-rotor platform can only reveal the second-order time-delay τ_2 with additional stability augmentation system simply because it is too fast. From the small quad-rotor shown in Fig. 1, 10 % of r_2 input in roll or pitch axis yields 200~250°/s/s angular acceleration because the moment of inertia is very small.

A systematic and analytic process to implement the cascaded attitude control is thus proposed as summarized with a process diagram in Fig. 4. Each blocks have the name of the step on the top side and key notes on the bottom side.

The first problem of the safety issue is solved by having P control in the secondary control C_2, and an automated frequency sweep input. The first process, the 'auto-commanded test for secondary loop', initiates a frequency sweep with C_1 control being turned off which is only possible in a very short time. Therefore, the use of 'P-only' control in C_2 still needs

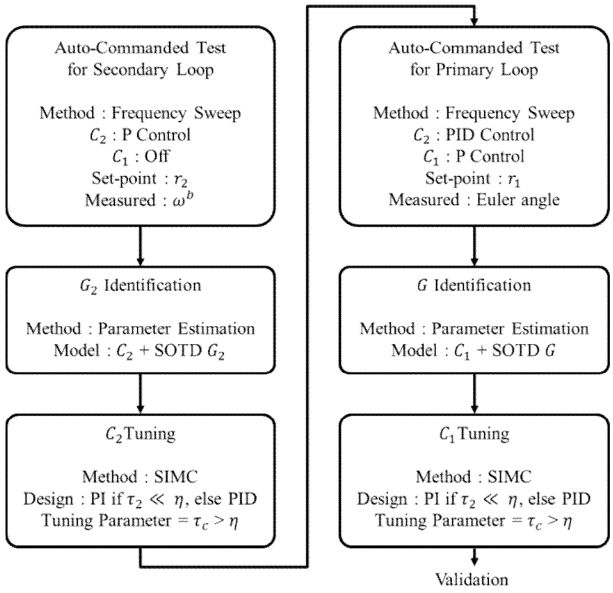

Fig. 4. Proposed procedure of implementing the cascaded attitude control.

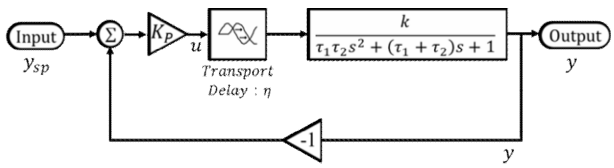

Fig. 5. Simulink model for parameter estimation.

an automated control input. The automated input has been used widely in automatic control tuning methods where it is commonly practiced with a relay switch input – see Ref. [34]. The automated control input not only provides a safer testing environment, but also the reproduction of the same input-output response data.

Since the sweeping value from the first process is the secondary control set-point r_2 - not the actuator control signal u - the second process of 'G_2 identification' is initiated with the parameter estimation method which optimizes the parameters with certain optimization method instead of the system ID method that can only optimize the input-output transfer function. In this research, MATLAB-Simulink® is used, where the Simulink® model of C_2 and G_2 is created as illustrated in Fig. 5, and four unknown parameters of k, τ_1, τ_2 and η were identified with the Parameter Estimation Toolbox®.

After the SOTD G_2 is identified, the SIMC method can be applied in the next step of 'C_2 tuning', where the value of τ_2 determines the option between PI and PID control, and all control parameters of Eqs. (9a)-(9c) can be determined with a single tuning parameter τ_c. It is already mentioned that τ_1 does not have to be exact, but the ratio of τ_1 / k is required to be converged.

The whole process applied for the secondary loop is then repeated for the primary loop. However, the measured vari-

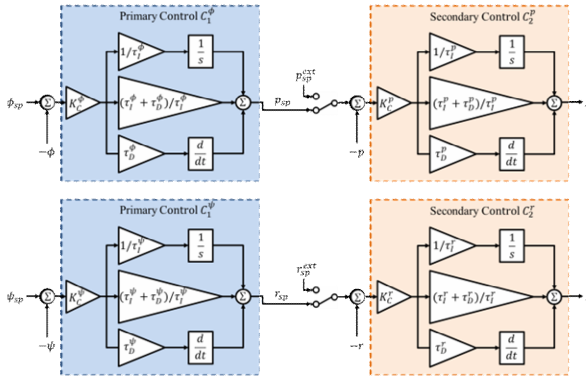

Fig. 6. Cascaded attitude control structure.

able for primary loop is not the secondary measured variable ω^b, but Euler angles this time. Since it is aimed to capture the linear response of $\boldsymbol{G}$, the secondary control is turned on with the PI or PID control determined from the previous process. Using this scheme, the model uncertainty is reduced from another system identification, but the complexity is not increased due to the use of SIMC method. It will be shown through the exemplary application of the proposed process on a small quad-rotor UAV that the proposed method can effectively implement the cascaded attitude control.

3. Details and evaluation of proposed procedure

3.1 The applied control architecture

Fig. 6 shows the applied control architecture. Sometimes the series-form PID of Eq. (4) is also referred to a cascade PID, but it should not be confused with the cascade control. Eq. (4) is expressed in an interacting form, but it can also be expressed in an equivalent non-interacting form as:

$$C(s) = K_c\left(\frac{\tau_I + \tau_D}{\tau_I} + \frac{1}{\tau_I s} + \tau_D s\right) \tag{10}$$

where it can easily be seen that Eq. (10) is the same as a parallel-form PID, and conversion to ideal-form PID is a trivial task [32]. In this application, the roll, pitch and yaw attitude controls were implemented with proposed method, but because the roll and pitch are symmetric, only the cascaded roll and yaw controllers are illustrated in Fig. 6. Comparing with the general form of the cascade control system in Fig. 2, C_1 and C_2 are expressed in Fig. 6. Control parameters are distinguished by the name of the measured variable – ϕ, p, ψ and r. The subscript sp indicates the signal is a set-point, and the superscript ext indicates the external control signal for independent operation of secondary loop while the primary control is turned off. From the secondary control of p, the control signal u is the *AIL*, the normalized rolling moment control input, and similarly, the *RUD* from the r control.

Prior to commissioning the proposed process, it is assumed that an initial gain values are provided because the flying vehicle has to fly in order to acquire any data unless an adequate ground test facility is incorporated. Therefore, the provided initial gain values are assumed to be acquired from empirical tuning process which should provide an initial set of 'safe gain' values. In practice, initial gain values were manually tuned with following simple rules prior to beginning the proposed process.

(1) Increasing the K_C decreases rising time.
(2) Increasing the τ_D improves stability.
(3) Starting from large value of the τ_I, error decays faster by decreasing the τ_I.
(4) Decreasing the τ_I decreases stability.

However, for very first gain values, the τ_I was set to $\tau_I = \infty$ and $\tau_D = 0$, which results to a P-P control. Because the secondary control is naturally a derivative action of the primary control, the resulting P-P control is equivalent to a single-loop PD control with set-point weighting modification to eliminate the 'derivative kick' from set-point changes – see Appendix A.2.

3.2 Auto-commanded test for secondary loop

From this first process, different methods of signal inputs were compared. It was first considered to use an open-loop doublet command for the *AIL* and *RUD*. Fig. 7 shows the results of p and r responses from multiple tests. The doublet input was automatically initiated when the body axis translational velocity is less than 0.1 m/s, ϕ and ψ are less than 3 deg, p and r are less than 1°/s, which corresponds to a nearly-trimmed state. It was tested with roll controls turned off for 0.85 seconds, and yaw controls turned off for 5.8 seconds, but only with the scheduled doublet input of respective *AIL* and *RUD*.

It can be seen from Fig. 7 that responses are very different for two cases because the quad-rotor platform was very susceptible to wind, and it was not possible to maintain the uncontrolled state. Therefore, it was concluded that no good data can be achieved with a doublet u input. A frequency sweep and 3-2-1-1 input could also lead to a catastrophic result from an open-loop excitation.

Therefore, the secondary control was incorporated with a P-only control as shown in Fig. 5. The set-point of p_{sp}^{ext} and r_{sp}^{ext} each were excited with a signal with the form:

$$y_{sp} = A\sin\left(2\pi f t\right) \tag{11}$$

where A is amplitude and f is frequency which is changing from low frequency to high frequency.

Fig. 8 shows the frequency sweep results of p and r responses. For the p response, pre-scheduled frequency sweep was automatically given to p_{sp}^{ext} with a termination condition that switches back to normal operating state when the plat-

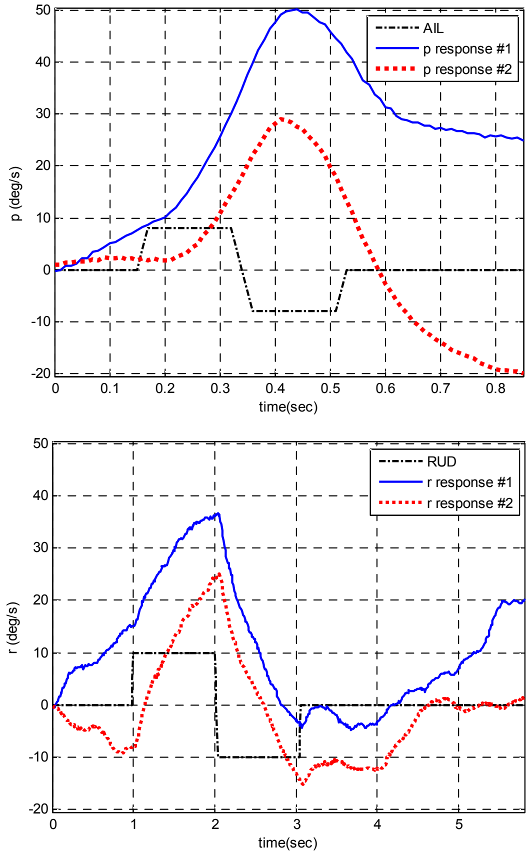

Fig. 7. Response from a doublet command for *AIL* and *RUD*.

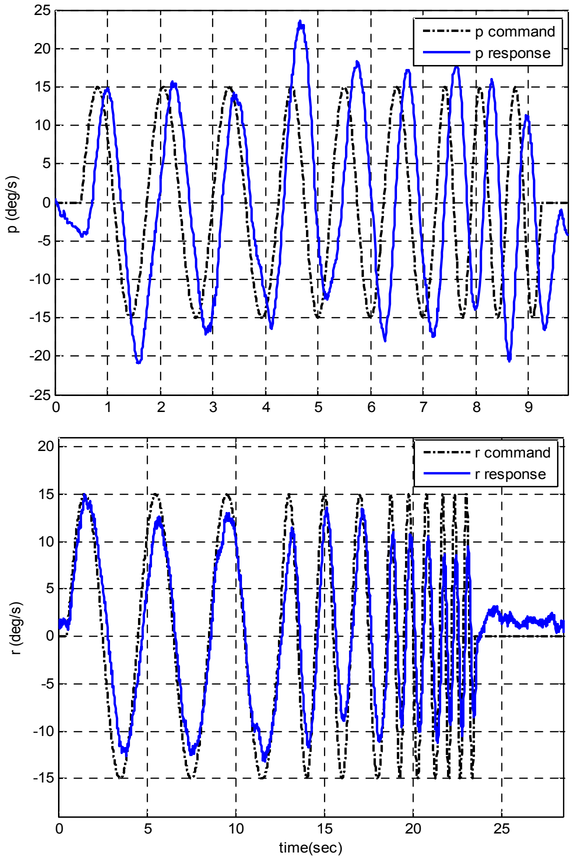

Fig. 8. Response from a frequency sweep command for p_{sp}^{ext} and r_{sp}^{ext}.

form's angle ϕ drifts beyond the limit of 20°. The choice of amplitude A was 15°/s which was thought to have enough Signal-to-noise (SN) ratio but small enough to avoid the termination condition. The frequency f was stepping 0.8, 1.0 and 1.5 Hz after three sine waves were repeated. For r_{sp}^{ext} input to r response, A was also 15°/s, but f was stepping 0.25, 0.5 and 1.0, where the stepping frequencies were adjusted to start from lower frequency because the yaw axis is not incorporated with translational acceleration.

Using the closed-loop automated frequency-sweep method, the required data for system identification were acquired safely. Moreover, the response data had higher-quality information than a doublet input because the frequency sweep naturally removes the effect of initial condition after a couple of sine waves. It is also noteworthy that some researchers have already argued that the closed-loop system identification provides more accurate identification of the model. Hjalmarsson et al. have shown that when the open-loop identification and closed-loop identification is compared, the more accurate model can be achieved using the closed-loop identification especially when the model is perturbed by noise [35]. Harun-Or-Rashid et al. have demonstrated the use of a PID control fully included in the parameter estimation of a coaxial-rotor helicopter model for a 6-DOF non-linear system identification [36].

3.3 G_2 identification

To apply SIMC tuning-rule directly, it was avoided to use the general system identification method that yields a higher-order transfer function [19], but the Parameter Estimation Toolbox® of MATLAB-Simulink® was used. Using the parameter estimation method, the dead-time η could be modeled with a 'transport delay' block that serves as a pure delay, and the complete Simulink® model was shown in Fig. 5.

Parameter estimation was performed with the genetic-algorithm-based optimization method. The genetic algorithm avoids the problem of local minimum solution by reproduction, crossover, and mutation, where other methods such as a gradient decent and nonlinear least squares often falls into a local minimum depending on the initial parameter value [36, 37]. Fig. 9 shows the result of parameter estimation for x^b-axis angular velocity p, and the result of validation. Although the response data were affected by external wind, it can be seen that the closed-loop method kept the effect within a small magnitude to yield a model with a reasonable accuracy.

Fig. 10 shows the result of parameter estimation for z^b-axis angular velocity r, and the result of validation. Because r dynamics is not affected by translational acceleration, and slower dynamics allowed more variation of frequencies, the identification result of the r dynamics shows better agree-

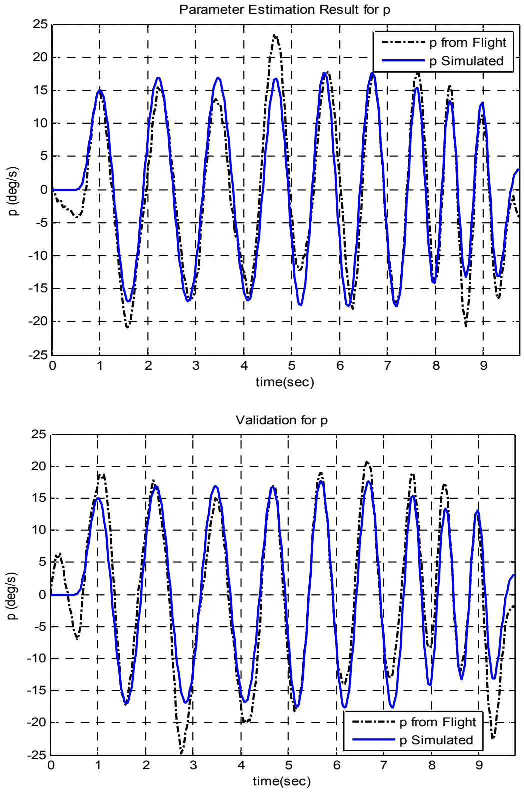

Fig. 9. Parameter estimation and validation results for p.

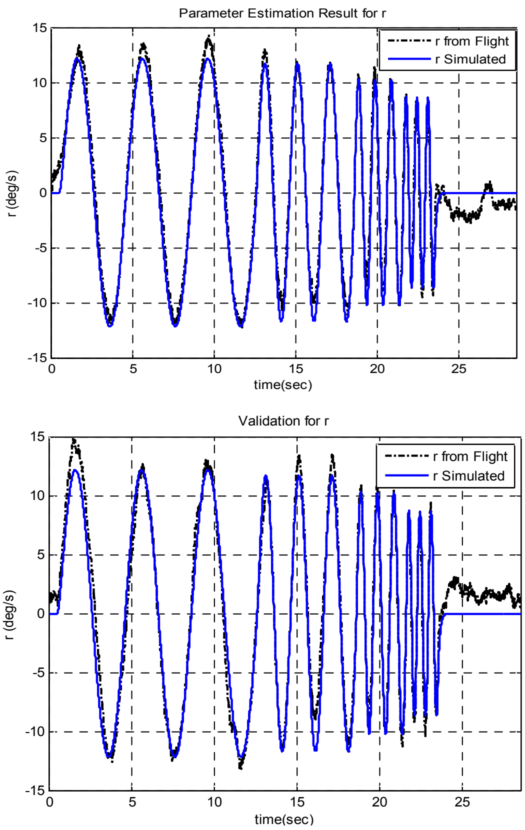

Fig. 10. Parameter estimation and validation results for r.

Table 1. Identified G_1.

Mode	Parameter	Value for SOTD	Value for FOTD (If used)
p dynamics for secondary control C_2^p	k^p	47.682	-
	τ_1^p	1.280	-
	τ_2^p	0.133	-
	η^p	0.020	-
r dynamics for secondary control C_2^r	k^r	3.328	3.328
	τ_1^r	0.752	0.754
	τ_2^r	0.004	-
	η^r	0.010	0.018

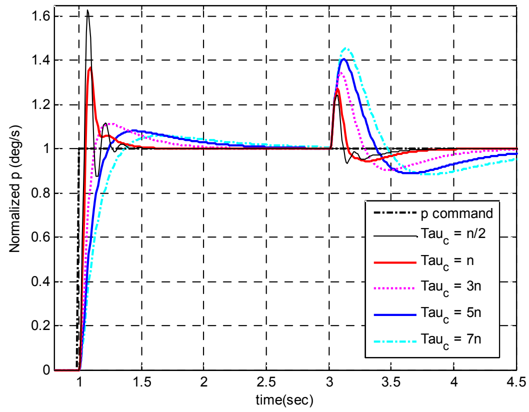

Fig. 11. Simulated p responses from step input and load disturbance with various τ_c^p.

ment than that of the p dynamics.

The resultant SOTD G_2 parameters are summarized in Table 1. In case of r dynamic mode, τ_2^r was much smaller than η^r, thus it can be reduced to the FOTD model with a well-known Half-Rule [10, 25, 32]. Table 1 also includes the FOTD model for r dynamics.

3.4 C_2 tuning

From the parameters of Table 1 and the SIMC tuning-rules in Eqs. (9a)-(9c), secondary control C_2 parameters can be determined. The benefit of the SIMC tuning-rule is that it converts the PID-tuning problem to a single parameter tuning problem of τ_c, the time constant of desired optimum response. Smaller value of τ_c leads to faster response but greater τ_c leads to better robustness [32].

As this research contains the problem of uncertain process model, it is followed the evaluation of SIMC method for various examples of process models by Skogestad [32, 38]. The recommended choice of $\tau_c = \eta$ is the optimum point if output performance criteria such as Integrated absolute error (IAE), rising and settling time are applied for a step response and a load disturbance. The robustness is also known to

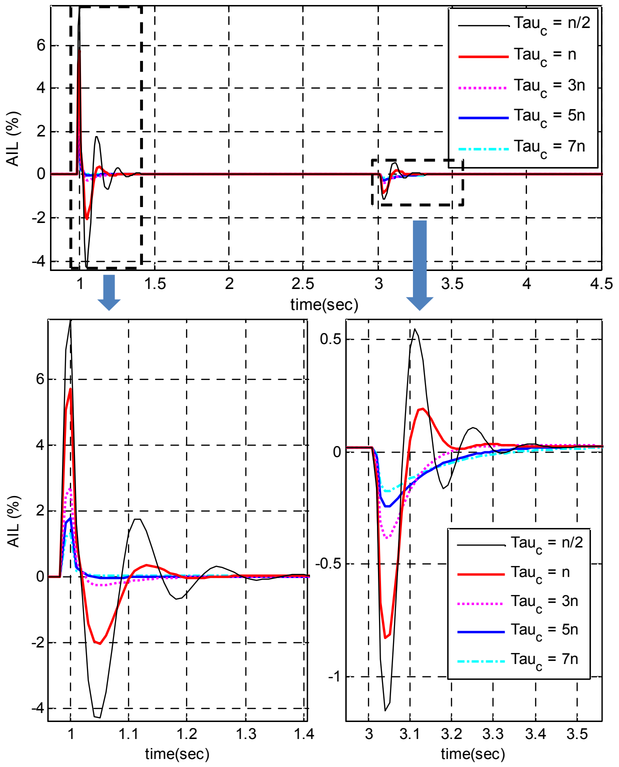

Fig. 12. Input usage from the previous simulation.

achieve Maximum sensitivity (M_s) value near or less than 1.7 for various process models including 4th and 5th order lag-dominant models. If $M_s < 1.7$, the Gain margin (GM) and Phase margin (PM) are always GM > 2.43 and PM > 34.2°, respectively, and these margins are accepted as a suggested robustness margins. Even when compared with other PID tuning methods, it was shown that the SIMC method has good performance and robustness [32]. Since greater τ_c was shown to increase robustness, it is sufficient to say that the τ_c value being $\tau_c > \eta$ provides a good robustness up to the maximum value $\tau_{c,max}$ [33], but $\tau_{c,max}$ is not readily defined for a small flying vehicle yet.

Simulated tests were performed for various values of τ_c with identified p dynamics in Table 1. For η = 0.02 and τ_c value changing from $\eta/2$ up to 7η , a step input was given at 1.0 s, and an input load disturbance was given at 3.0 s. The resultant response is shown in Fig. 11, and the control input usage, where it is *AIL* in this case, is shown from Fig. 12 with an additional subplots for regions of interest. The decreased τ_c from η (τ_c = 0.5η case) clearly shows a large overshoot, oscillation, and excessive use of control input. With SIMC setup of $\tau_c = \eta$, there was some overshoot and oscillation from step input but it showed an excellent load disturbance rejection. However, as the τ_c increased, the Fig. 12 shows that input usage was much decreased.

Even though the well-established methodology is adopted, the fundamental problems, when the SIMC method is applied to a real UAV system, are the saturated input and the sensor that acquires the state data. The evaluation of control methods are usually performed with a normalized set-point and state values, and a general linear analysis doesn't account for a large magnitude of error between set-point and state value which easily saturates the control signal to ± 100 % limit and resultant response to the limit of sensors ranges. Therefore, in this research, the τ_c value was tuned for a better input performance, where the input performance indicates the manipulated input usage, and can be measured by the Total variation (TV):

$$\mathrm{TV} = \int_{t=0}^{\infty} |u'| \, dt. \tag{12}$$

The TV should be as small as possible while maintaining a good output performance. From this C_2 tuning process, the evaluation of input performance helped tuning the τ_c for reduced likeliness of saturated input. It will be shown from the C_1 tuning process that the evaluation of input performance can reduce the likeliness of exceeding sensor ranges.

Table 2. Measured performance parameters from the simulation.

Section		TV	IAE	Max u
0.00 s ~ 2.99 s (Step input)	$\eta/2$	46.6	0.0814	7.92 %
	η	24.3	0.0799	5.74 %
	3η	9.43	0.115	2.72 %
	5η	5.79	0.153	1.78 %
	7η	4.20	0.185	1.32 %
3.00 s ~ 6.00 s (Load disturbance)	$\eta/2$	5.35	0.0292	0.525 %
	η	2.80	0.0415	0.172 %
	3η	1.10	0.103	0.00774 %
	5η	0.707	0.165	0.00354 %
	7η	0.519	0.225	0.00191 %

The resultant measures of TVs are shown from Table 2 where the IAE and maximum input *u* (*AIL*) were also measured for comparison. For τ_c being up to 7η , the value of TV decayed fast, but at the same time the IAE also increased. Since there was 76 % decrease of TV, 70 % decrease of maximum *u*, it was compensated with τ_c = 5η for final application for the C_2^p controller.

From similar effort, the C_2^r controller also had τ_c value near 5η , but because of small τ_2 value, the identified SOTD model was reduced to FOTD model as shown in Table 1, and the resulting C_2^r is a PI control. The final gain values are listed in Table 3.

Before moving on to the next process, it was tested with a step-input flight experiment for an intermediate validation. Fig. 13 shows the response of the C_2^p controller and the input *AIL* usage, and Fig. 14 shows the C_2^r response and the *RUD* usage. The state values are normalized from the real set-point value of 15°/s. The rising time of 0 to 100 % was 0.2 sec for

Table 3. Resultant gain setting for secondary controllers.

Controller	Parameter	Value
Secondary control C_2^p for p (PID)	τ_c^p	0.1
	k_c^p	0.224
	τ_I^p	0.480
	τ_D^p	0.133
Secondary control C_2^r for r (PI)	τ_c^r	0.1
	k_c^r	1.93
	τ_I^r	0.470
	τ_D^r	0

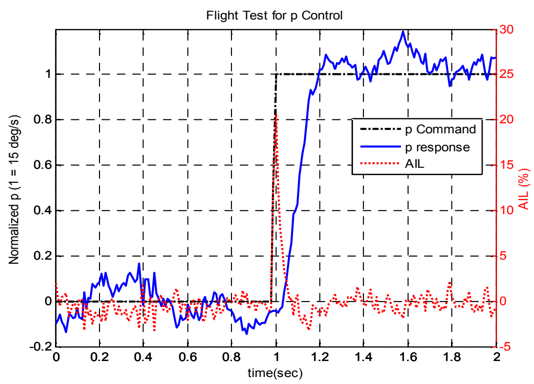

Fig. 13. Experimental validation of *p* control.

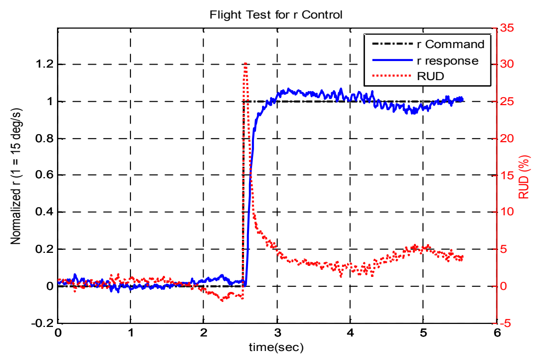

Fig. 14. Experimental validation of *r* control.

the C_2^p, and 0.3 s for that of the C_2^r. The responses have shown a convergence to set-point with good damping and moderate use of input u.

3.5 Auto-commanded test for primary loop

In this process, the same method from the first process was applied. The process model is the ***G***, which was shown from Fig. 2 to include closed-loop response of C_2 and G_2 with additional G_1. The C_1 control was also applied with P-only control. Fig. 15 shows the responses from the frequency sweep of ϕ_{sp}^{ext} and ψ_{sp}^{ext}. Since respective secondary controllers of C_2^p and C_2^r have been tuned with SIMC method, the responses no longer had a significant affect from external wind.

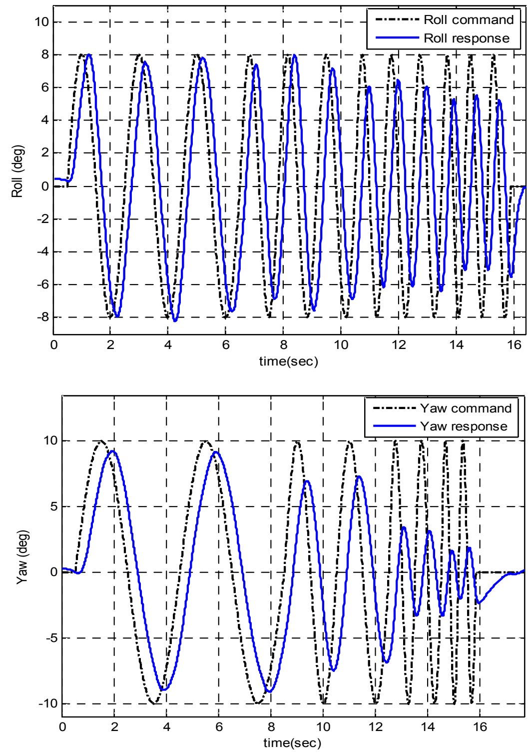

Fig. 15. Response from a frequency sweep command for ϕ_{sp}^{ext} (roll) and ψ_{sp}^{ext} (yaw).

3.6 G identification

Since the linear response of closed-loop ***G*** and C_1 is to be measured for identification of SOTD model of ***G***, which is the same as the G_1 identification process, the same Simulink® model as shown in Fig. 5 was applied - that is, no detailed models of previously identified G_2 and C_2 are explicitly included in ***G***.

The identified parameters are listed in Table 4, and the responses of the resultant models are shown in Fig. 16. Notice that the value τ_2 for both G^ϕ and G^ψ is much smaller than the respective dominant-lag time constant of τ_1, which means that the SOTD can be reduced to FOTD model. However, the closed-loop ***G*** has different characteristic that there is no explicit dead-time, and the parameter estimation will result to η value being close to zero. Therefore, the value of η was forced to the half of 100 Hz discrete sampling period, thus $\eta =$ 0.005. In this situation, the τ_2 is greater than 8η, and the SOTD model was used.

3.7 C_1 tuning

The cascaded attitude control requires a consideration of a real physical sensor. Current state-of-the-art AHRS sensors

Table 4. Identified ***G***.

Controller	Parameter	Value
Secondary control C_2^p for p (PID)	τ_c^p	0.1
	k_c^p	0.224
	τ_I^p	0.480
	τ_D^p	0.133
Secondary control C_2^r for r (PI)	τ_c^r	0.1
	k_c^r	1.93
	τ_I^r	0.470
	τ_D^r	0

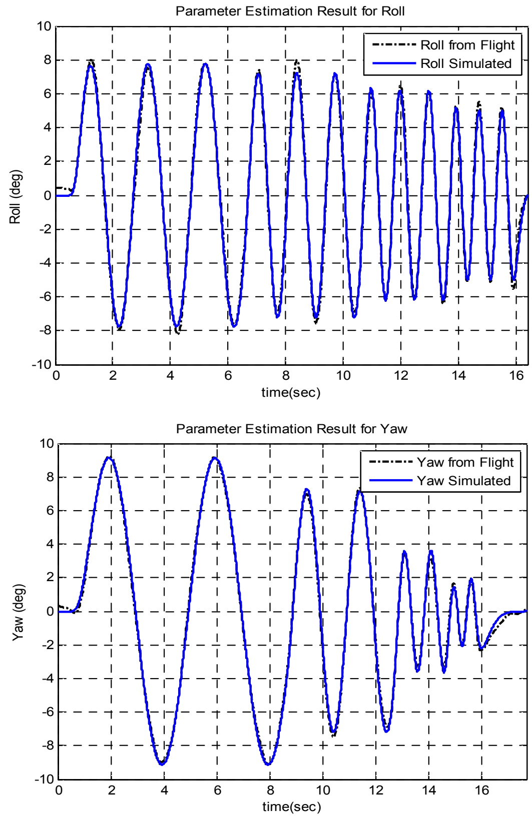

Fig. 16. Parameter estimation and results for ϕ and ψ .

have the angular velocity specification ranging from 250°/s to 3000°/s [39], but it is assumed that the minimum specification of a low-cost AHRS sensor is 360°/s. In order to avoid exceeding the maximum measurable angular velocity, the maximum value for set-point r_2 should be limited below 250°/s when 40 % overshoot is considered. Since it only takes 0.36 s to reach 90° with 250°/s of angular velocity, and 0.08 s to reach 20° with that angular velocity, 250°/s is sufficiently fast angular velocity for a real application on a non-aggressive maneuver UAV. In fact, for a small UAVs with its components not rigidly attached, exceeding 250°/s may not guarantee

Table 5. Measured performance parameters from the simulation.

Section		TV	IAE	Max *u*
0.00 s ~ 5.99 s (Step input)		3410	2.62	250°/s
		764	3.55	250°/s
	0.20	479	6.03	183°/s
	0.30	320	8.88	129°/s
	0.40	249	11.5	99.3°/s
6.00 s ~ 13.00 s (Load disturbance)		3100	0.0285	141°/s
		133	0.506	0.761°/s
	0.20	66.5	1.06	0.365°/s
	0.30	44.3	1.60	0.239°/s
	0.40	33.5	2.13	0.177°/s

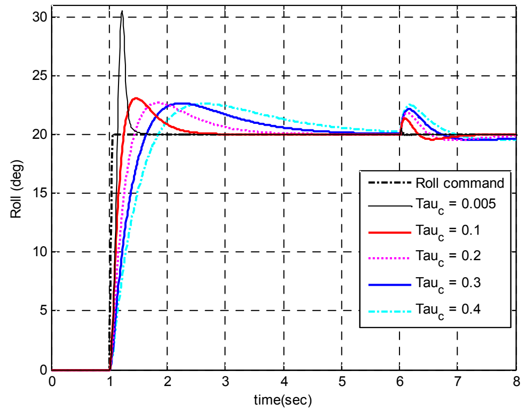

Fig. 17. Simulated ϕ responses from step input and load disturbance with various τ_c^ϕ .

the structural integrity. Therefore, the application of SIMC method on a primary control of a cascaded attitude control requires a different approach from a conventional linear system design way.

From this research, it is suggested that an analysis of step input with real physical value should be performed. Moreover, as it was suggested from the C_2 tuning process, input performance should be carefully examined in order to determine the value of τ_c . It is simulated with various τ_c^ϕ and saturation limit of 250°/s for the primary controller C_1^ϕ . The output responses of G^ϕ are shown from Fig. 17 where the 20° step input starts from 1.0 s, and a load disturbance is given at 6.0 s. For a case where the effective delay η is very small, setting the $\tau_c = 0.005$ resulted in a large overshoot of 50 % from the step input, and at least 10 η was required before the overshoot settled down to a low value. The current model which has a large dominant lag time constant τ_1 settles at around 10 % of overshoot regardless of increased τ_c , but the affect from load disturbance was steadily increasing. However, it is more important to evaluate the input performance, where the simulated data of manipulated input usage is shown from Fig. 18, and various performance parameters are summarized in Table 5.

Table 6. Resultant gain setting for primary controllers.

Controller	Parameter	Value
Secondary control C_2^p for p (PID)	τ_c^p	0.1
	k_c^p	0.224
	τ_I^p	0.480
	τ_D^p	0.133
Secondary control C_2^r for r (PI)	τ_c^r	0.1
	k_c^r	1.93
	τ_I^r	0.470
	τ_D^r	0

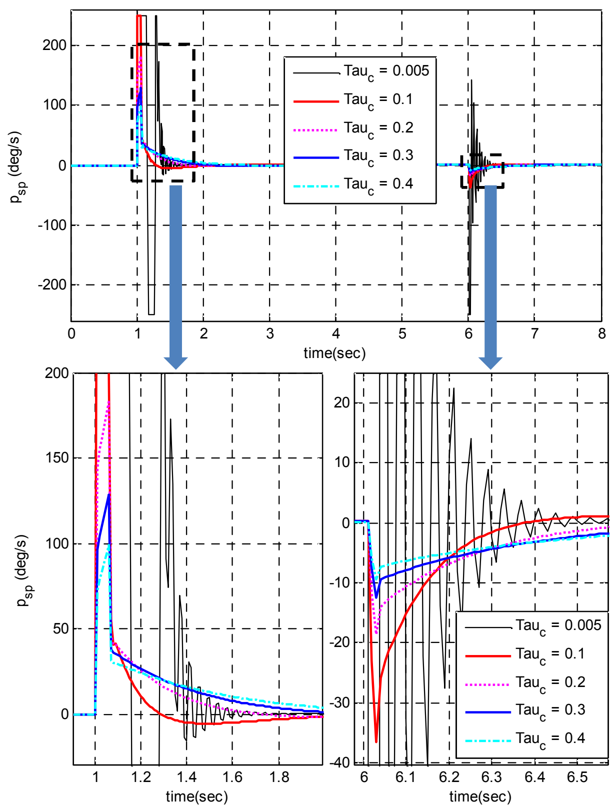

Fig. 18. Input usage from the previous simulation.

The use of SIMC PID setting of $\tau_c =$ 0.005 results to an extremely large TV while the IAE is smallest. However, up to $\tau_c =$ 0.1, the maximum input was saturating to the limit of 250°/s, thus it was considered that $\tau_c > 0.15$ should be used. The final choice was $\tau_c =$ 0.3, and using it, the maximum u is 129°/s, which is nearly half the value from 250°/s, while TV is decreased by 90 %.

3.8 Validation

The final set of C_1 controller parameters are listed in Table

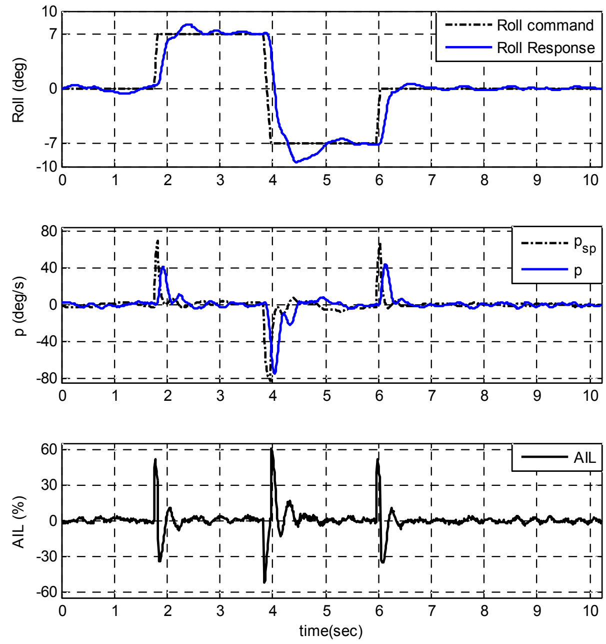

Fig. 19. Flight experiment data of a doublet-roll command.

6. Along with C_2 controller parameters shown from Table 3, all PID gain values were implemented to the cascaded attitude controller shown from Fig. 6. The saturation limit was applied with 300°/s for p_{sp}, the set-point for secondary loop of the roll controller. However, the saturation limit was applied with 100°/s for r_{sp}, the set-point for secondary loop of the yaw controller, because the bandwidth of the magnetometer-based heading reference system is much slower in yaw axis than the roll axis. Therefore, the yaw angle should generally be maintained with slower angular velocity. Notice that in the Table 6, it is also further increased with τ_c^{ψ} value being 0.4, while τ_c^{ϕ} is 0.3, for the purpose of slower control.

The final validations of roll and yaw control were performed with a non-aggressive doublet maneuver to minimize cumulated velocity because the step maneuver accelerates the UAV to one direction. For roll control, a 7° doublet set-point was given, and Fig. 19 shows the result of the primary control, secondary and *AIL* input. There was maximum of 16 % overshoot for roll angle, and the maximum p_{sp} of 80°/s was given for the secondary control. The maximum *AIL* was 60 %. Fig. 20 shows the yaw control test result where a 10° doublet set-point was given. Maximum of 12 % overshoot was observed due to more robust setting, and the maximum r_{sp} of 40°/s was given for the secondary control. The maximum *RUD* was 50 %, but notice that *RUD* is much decreased if integrated elements are removed. Since all of the PID controller are represented in a non-interacting form, the Proportional (P) elements and Integral (I) elements were separately recorded, and as it is shown from Fig. 21, the maximum P element of RUD is 35 %. This means that both the input usage of r_{sp} and *RUD* are almost halved from that of p_{sp} and *AIL*.

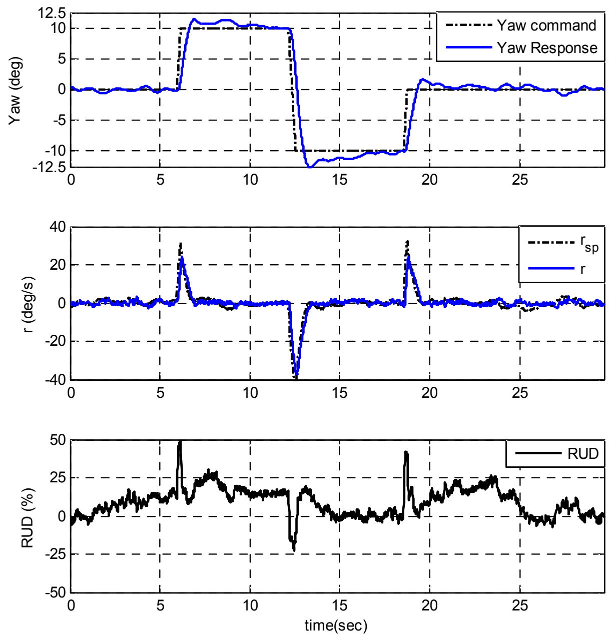

Fig. 20. Flight experiment data of a doublet-yaw command.

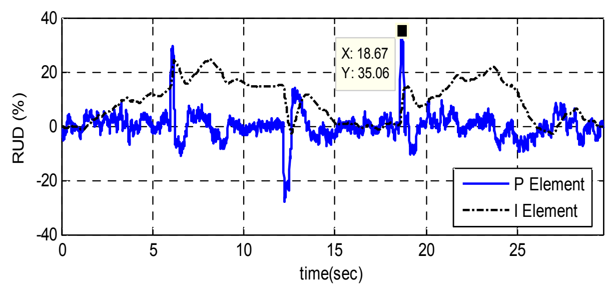

Fig. 21. Proportional and Integral element of *RUD*.

4. Conclusions

It was confirmed from the experimental validation that currently proposed method of applying the cascaded control system to the attitude control of a VTOL UAV was successfully implemented to a small quad-rotor UAV with 3.9 kg weight. It was found that, using the SIMC method, the cascaded control structure could be managed with fundamentally by only two τ_c parameters – the τ_c for each of the primary and secondary controller. The relatively small value of τ_c in the secondary loop realized a faster response and a good load disturbance rejection, while the larger value of τ_c in the primary loop allowed the compensation between the output and input performance to limit the control speed within safe region.

Moreover, the system identification process could be realized for a small quad-rotor UAV without any ground test-bed, but by allowing the P-only control and optimizing the SOTD model parameters directly to the set-point frequency sweep data acquired from the flight test. This paper summarized the process of applying the cascaded attitude control from Fig. 4, and all of processes were evaluated from multiple applications of the roll and the yaw control, where the yaw axis had much smaller secondary lag, and the magnetometer-based heading reference system only allowed about one-third of angular velocity in the yaw rate than the roll rate.

For more lessons learned, it was found that:

- The cascaded attitude control allowed more physical insight for attitude control because the angular velocity could directly be managed. The cascade not only provide a tighter and better load disturbance rejection, but also provides an explicit performance regulation for the intermediate signal. From this benefit, it was possible to safely limiting the angular velocity of the yaw control within the measurable region of yaw rate prior to flight experiment. For a single-loop control, this kind of regulation can only be achieved from giving up the tight control because the secondary measured variable of angular velocity is not explicitly present.
- The SIMC method could not be applied without modification for cascaded control because of the large manipulated input usage. Therefore, the TV should be the yardstick for tuning the secondary control, and the maximum u should the yardstick for tuning the primary control in addition to the TV, while the IAE still needs to be maintained within small value.
- The debatable structure of PID problem in cascade control system was solved by using the SIMC method that consolidated the IMC and direct-synthesis method. Therefore, it is the second-order lag time constant τ_2 that determines PID structure, and the full PID-PID was possible without any additional modification with set-point weighting.
- Although the anti-windup problem was not discussed because there should be no problem during flight, however, it was required that gains should be scheduled to have all $\tau_I = \infty$ on the ground due to the PID-PID structure. If the anti-windup is not considered at all, the UAV may flip over as soon as the throttle is raised.

Acknowledgment

This work was supported by the National Research Foundation of Korea (NRF) grant funded by the Korea government (MSIP) (No. NRF-2015R1A2A2A01005494). This work was also supported by the Human Resource Training Program for Regional Innovation and Creativity through the Ministry of Education and National Research Foundation of Korea (NRF-2015H1C1A1035499).

References

[1] S. J. Zaloga, D. Rockwell and P. Finnegan, *World Unmanned Aerial Vehicle Systems: Market Profile and Forecast,* 2011 Ed., Teal Group Corporation, Fairfax, Virginia (2011).

[2] K. J. Åström and T. Hägglund, The future of PID control, *Control Engineering Practice*, 9 (11) (2001) 1163-1175.

[3] C. S. Lee and R. V. Gonzalez, Fuzzy logic versus a PID con-

troller for position control of a muscle-like actuated arm, *Journal of Mechanical Science and Technology*, 22 (8) (2008) 1475-1482.

[4] R. C. DeMott II, Development of a flexible FPGA-based platform for flight control system research, *M.S. Thesis*, Virginia Commonwealth University, Richmond, Virginia (2010).

[5] H. Y. Chao, Y. C. Cao and Y. Q. Chen, Autopilots for small unmanned aerial vehicles: a survey, *Int. J. of Control, Automation, and Systems*, 8 (1) (2010) 36-44.

[6] T. Liu and F. Gao, *Industrial Process Identification and Control Design*, Springer, London, UK (2012).

[7] P. R. Krishnaswamy, G. P. Rangaiah, R. K. Jha and P. B. Deshpande, When to use cascade control, *Industrial & Engineering Chemistry Research*, 29 (10) (1990) 2163-2166.

[8] R. Czyba and G. Szafranski, Control structure impact on the flying performance of the multi-rotor VTOL platform - design, analysis and experimental validation, *Int. J. of Advanced Robotic System*, 10 (62) (2013) DOI: 10.5772/53747.

[9] B. Godbolt and A. F. Lynch, A novel cascade controller for a helicopter UAV with small body force compensation, *Proc. of American Control Conference, IEEE*, Washington, DC, USA (2013) 800-805.

[10] K. J. Åström and T. Hägglund, *Advanced PID Control*, International Society of Automation, Research Triangle Park, NC, USA (2006).

[11] A. Soumelidis et al., Control of an experimental mini quadrotor UAV, *Proc. of Control and Automation, 2008 16th Mediterranean Conference on. IEEE*, Ajaccio, France (2008) 1252-1257.

[12] P. Castillo, R. Lozano and A. E. Dzul, *Modelling and control of mini-flying machines*, Springer (2006).

[13] R. G. Franks and C. W. Worley, Quantitative analysis of cascade control, *Industrial & Engineering Chemistry*, 48 (6) (1956) 1074-1079.

[14] I. Kaya, Improving performance using cascade control and a Smith predictor, *ISA Transactions*, 40 (3) (2001) 223-234.

[15] Y. Lee, S. Park and M. Lee, PID controller tuning to obtain desired closed loop responses for cascade control systems, *Industrial & Engineering Chemistry Research*, 37 (5) (1998) 1859-1865.

[16] B. Polajžer et al., Decentralized PI/PD position control for active magnetic bearings, *Electrical Engineering*, 89 (1) (2006) 53-59.

[17] W. Tan, J. Liu, T. Chen and H. J. Marquez, Robust analysis and PID tuning of cascade control systems, *Chemical Engineering Communications*, 192 (9) (2005) 1204-1220.

[18] M. B. Tischler, System identification methods for aircraft flight control development and validation, *NASA Technical Memorandum 110369 and USAATCOM Technical Report 95-A-007*, USA (1995).

[19] O. Nelles, *Nonlinear system identification: from classical approaches to neural networks and fuzzy models*, Springer-Verlag, Berlin, Germany (2001).

[20] P. G. Hamel and J. Kaletka, Advances in rotorcraft system identification, *Progress in Aerospace Sciences*, 33 (3) (1997) 259-284.

[21] J. Suk, Y. Lee, S. Kim, H. Koo and J. Kim, System identification and stability evaluation of an unmanned aerial vehicle from automated flight tests, *KSME International Journal*, 17 (5) (2003) 654-667.

[22] M. R. Endsley, The application of human factors to the development of expert systems for advanced cockpits, *Proc. of the Human Factors and Ergonomics Society Annual Meeting*, New York, USA (1987) 1388-1392.

[23] R. K. Mudi and N. R. Pal, A robust self-tuning scheme for PI-and PD-type fuzzy controllers, *Fuzzy Systems, IEEE Transactions on*, 7 (1) (1999) 2-16.

[24] J. G. Ziegler and N. B. Nichols, Optimum settings for automatic controllers, *Trans. ASME*, 64 (11) (1942) 759-765.

[25] K. J. Åström and T. Hägglund, Revisiting the Ziegler–Nichols step response method for PID control, *Journal of Process Control*, 14 (6) (2004) 635-650.

[26] A. Visioli and Q. C. Zhong, *Control of Integral Processes with Dead Time*, Springer-Verlag, London, UK (2011).

[27] E. Poulin and A. Pomerleau, PID tuning for integrating and unstable processes, *Control Theory Appl.*, 143 (5) (1996) 429-435.

[28] C. E. Garcia and M. Morari, Internal model control. A unifying review and some new results, *Industrial & Engineering Chemistry Process Design and Development*, 21 (2) (1982) 308-323.

[29] C. S. Jung, H. K. Song and J. C. Hyun, A direct synthesis tuning method of unstable first-order-plus-time-delay processes, *Journal of Process Control*, 9 (3) (1999) 265-269.

[30] E. F. Jacob and M. Chidambaram, Design of controllers for unstable first-order plus time delay systems, *Computers & Chemical Engineering*, 20 (5) (1996) 579-584.

[31] D. E. Rivera, M. Morari and S. Skogestad, Internal model control: PID controller design, *Industrial & Engineering Chemistry Process Design and Development*, 25 (1) (1986) 252-265.

[32] S. Skogestad, Simple analytic rules for model reduction and PID controller tuning, *Journal of Process Control*, 13 (4) (2003) 291-309.

[33] S. Skogestad, Tuning for smooth PID control with acceptable disturbance rejection, *Industrial & Engineering Chemistry Research*, 45 (23) (2006) 7817-7822.

[34] K. J. Åström, T. Hägglund, C. C. Hang and W. K. Ho, Automatic tuning and adaptation for PID controllers-a survey, *Control Engineering Practice*, 1 (4) (1993) 699-714.

[35] H. Hjalmarsson, M. Gevers and F. De Bruyne, For model-based control design, closed-loop identification gives better performance, *Automatica*, 32 (12) (1996) 1659-1673.

[36] M. Harun-Or-Rashid et al., Unmanned coaxial rotor helicopter dynamics and system parameter estimation, *Journal of Mechanical Science and Technology*, 28 (9) (2014) 3797-3805.

[37] W. D. Chang, Nonlinear system identification and control using a real-coded genetic algorithm, *Applied Mathematical Modelling*, 31 (3) (2007) 541-550.

[38] S. Skogestad, Probably the best simple PID tuning rules in the world, *Proc. of AIChE Annual Meeting*, Reno, Nevada (2001).

[39] M. Cordero et al., Survey on attitude and heading reference

systems for remotely piloted aircraft systems, *2014 International Conference on Unmanned Aircraft Systems (ICUAS), IEEE*, Orlando, Florida, USA (2014) 876-884.

[40] J. B. Song, Y. S. Byun, J. Kim and B. S. Kang, Guidance and control of a scaled-down quad tilt prop PAV, *Journal of Mechanical Science Technology*, 29 (2) (2014) 807-825.

Appendix

A.1 The choice of control signals and the distributing matrix for quad rotor

It is followed a set of conventional control input terms widely used in aircraft control, i.e., the aileron, elevator, rudder, and throttle. Consider a quad-rotor represented in Fig. 1 that has four motors equivalently placed in distance l . Since the aileron is a control input to create a rolling moment, aileron (*AIL*) is defined from thrust (T_i , i = 1, 2, 3, 4) as :

$$AIL = a\left(T_3 + T_4 - T_1 - T_2\right) \times l \tag{A.1}$$

which is proportional to rolling moment. Similarly, the elevator (*ELE*) , rudder (*RUD*) and throttle (*THR*) are defined from thrust and torque (Q_i , i = 1, 2, 3, 4) as:

$$ELE = a\left(T_1 + T_4 - T_2 - T_3\right) \times l \ , \tag{A.2}$$

$$RUD = a\left(Q_2 + Q_4 - Q_1 - Q_3\right) = b(T_1 + T_4 - T_2 - T_3) \tag{A.3}$$

$$THR = \left(T_1 + T_2 + T_3 + T_4\right) \tag{A.4}$$

where the torque is assumed to be linearly proportional to the thrust, and all of *AIL, ELE, RUD, THR* can be represented by thrusts. After arranging input and thrust relations into matrix form and inversing it, all of four control inputs can then be mapped into each motors by following equation:

$$\begin{bmatrix} T_1 \\ T_2 \\ T_3 \\ T_4 \end{bmatrix} = \begin{bmatrix} -k_1 & k_1 & k_2 & 1 \\ -k_1 & -k_1 & -k_2 & 1 \\ k_1 & -k_1 & k_2 & 1 \\ k_1 & k_1 & -k_2 & 1 \end{bmatrix} \begin{bmatrix} AIL \\ ELE \\ RUD \\ THR \end{bmatrix} \tag{A.5}$$

where k_1 and k_2 are distributing gain constants. In this research, *AIL*, *ELE*, *RUD* are normalized into -100 ~ +100 %, and *THR* is normalized into 0~100 % from the available thrust depending on the motor. By normalizing it, we can have the same distributing constants regardless of the platform weight and motor thrust.

For the quad-rotor UAV used in this research, 100 % throttle creates total of 85 N thrust, and the hovering trim is around 45 % for 3.9 kg of mass. Since it is assumed that the UAV is operating at hovering condition, and available control force of 45 % margin is to be distributed to the *AIL*, *ELE* and *RUD*, 45 % throttle should be divided by 3. Therefore, for example, 100 % *AIL* should become 15 % throttle for each motor, and *AIL* should always be limited within 100 %.

A.2 Equivalent set-point weighting for initial cascade structure

The initial controller had only the proportional control in both of the primary and secondary loops (same as $\tau_I^p, \tau_I^r = \infty$, $\tau_D^p, \tau_D^r = 0$). This cascade controller of P-P form can be expressed in a single-loop PID control by time-domain input *u*:

$$u(t) = \left(K_c^P e(t) - \dot{y}(t)\right) K_c^S = K_c^P K_c^S \left(e(t) - \frac{K_c^S}{K_c^P} \dot{y}(t) \right) \tag{A.6}$$

where $e(t) = y_{sp}(t) - y(t)$. From Eq (A.6), it is clear that the proportional control action in the secondary loop is naturally a derivative action in the primary loop. Meanwhile, a general set-point weighting for a PID control can be expressed in time-domain as:

$$u(t) = K_C \left(\left(by_{sp}(t) - y(t)\right) + \tau_D \frac{d}{dt}\left(cy_{sp}(t) - y(t)\right) \right). \tag{A.7}$$

The resulting equation is the same as a single-loop PD control of Eq. (A.6) by substituting $K_C = K_C^P K_C^S$, $\tau_D = K_C^S / K_C^P$, and set-point weight of b = 1, $c = 0$ into Eq. (A.7). Alternatively, it is also called the PI-D control if an integral control is also associated. The PI-D control completely neglects the effect of dy_{sp} / dt term to remove 'derivative kick', and is widely used in practical applications of industrial control.

Jun-Beom Song received his Ph.D. degree in aerospace engineering from Pusan National University, Korea in 2015, and joined Dongwon Institute of Science and Technology, Korea, as a Professor at the same year. His research interests include guidance and control of an unmanned aircraft, and application of embedded systems. Since he is currently working in the Department of Aviation Maintenance, his interests also include the maintenance of manned or unmanned aircrafts, and how to train maintenance engineers with international standards of FAA and ICAO.

Beom-Soo Kang received his M.S. degree in aeronautical engineering from Korea Advanced Institute of Science and Technology, Korea in 1983. He received Ph.D. degree in mechanical engineering from University of California at Berkeley, California at 1990. He joined Pusan National University as a Professor since 1993. His research interests include unmanned aerial vehicle system, computer-aided engineering of manufacturing process by finite element method for structural analysis, materials processing and metal forming.